Inorganic Chemistry

Article

pubs.acs.org/IC

Mechanisms of Photoisomerization and Water-Oxidation Catalysis of Mononuclear Ruthenium(II) Monoaquo Complexes

Masanari Hirahara,[†] Mehmed Z. Ertem,[‡] Manabu Komi,[†] Hirosato Yamazaki,[†] Christopher J. Cramer,[‡] and Masayuki Yagi*[,†,§]

[†]Department of Materials Science and Technology, Faculty of Engineering, and Center for Transdisciplinary Research, Niigata University, 8050 Ikarashi-2, Niigata 950-2181, Japan

[§]Precursory Research for Embryonic Science and Technology (PRESTO), Japan Science and Technology Agency (JST), 4-1-8 Honcho, Kawaguchi, Saitama 332-0012, Japan

[‡]Department of Chemistry, Chemical Theory Center, and Supercomputing Institute, University of Minnesota, 207 Pleasant Street SE, Minneapolis, Minnesota 55455-0431, United States

Supporting Information

ABSTRACT: A ligation of Ru(tpy)Cl_3 (tpy = 2,2′:6′,2″-terpyridine) with 2-(2-pyridyl)-1,8-naphthyridine) (pynp) in the presence of LiCl gave *distal*-[Ru(tpy)(pynp)Cl]$^+$ (*d*-**1Cl**) selectively, whereas the ligation gave *proximal*-[Ru(tpy)-(pynp)OH_2]$^{2+}$ (*p*-**1H$_2$O**) selectively in the absence of halide ions. (The proximal/distal isomers were defined by the structural configuration between the 1,8-naphthyridine moiety and the aquo or chloro ligand.) An aquation reaction of *d*-**1Cl** quantitatively afforded *distal*-[Ru(tpy)(pynp)OH_2]$^{2+}$ (*d*-**1H$_2$O**) in water, and *d*-**1H$_2$O** is quantitatively photoisomerized to *p*-**1H$_2$O**. The mechanism of the photoisomerization was investigated by transient absorption spectroscopy and quantum chemical calculations. The temperature dependence of the transient absorption spectral change suggests existence of the thermally activated process from the ^{3}MLCT state with the activation energy (ΔE = 49 kJ mol^{-1}), which is close to that (41.7 kJ mol^{-1}) of the overall photoisomerization reaction. However, quantum chemical calculations suggest another activation process involving the conformational change of the pentacoordinated distal structure to the proximal structure. Quantum chemical calculations provide redox potentials and pK_a values for proton-coupled electron transfer reactions from Ru^{II}−OH_2 to Ru^{IV}═O in good agreement with experiments and provide an explanation for mechanistic differences between *d*-**1H$_2$O** and *p*-**1H$_2$O** with respect to water oxidation. The calculations show that water nucleophilic attack (WNA) on *d*-[**Ru^V−O**]$^{3+}$ (the ruthenyl oxo species derived from *d*-**1H$_2$O**, calculated $\Delta G^{\ddagger}$ of 87.9 kJ/mol) is favored over *p*-[**Ru^V−O**]$^{3+}$ (calculated $\Delta G^{\ddagger}$ of 104.6 kJ/mol) for O−O bond formation. Examination of the lowest unoccupied molecular orbitals in *d*- and *p*-[**Ru^V−O**]$^{3+}$ indicates that more orbital amplitude is concentrated on the [Ru−O] unit in the case of *d*-[**Ru^V−O**]$^{3+}$ than in the case of *p*-[**Ru^V−O**]$^{3+}$, where some of the amplitude is instead delocalized over the pynp ligand, making this isomer less electrophilic.

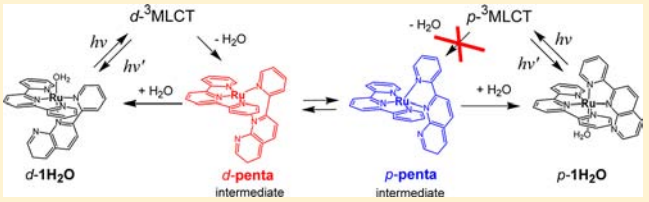

INTRODUCTION

The photochemical and photophysical properties of ruthenium(II) complexes with polypyridyl ligands have been extensively studied due to unique phenomena including photoluminescence,[1−3] photoredox,[1−3] photosubstitution,[4−6] and photoisomerization[7−10] processes typically involving a photoexcited triplet metal-to-ligand charge transfer (^{3}MLCT) state. With respect to the photoisomerization of polypyridyl ruthenium(II) aquo complexes, the photoisomerization of *cis*-[Ru(bpy)$_2$(OH_2)$_2$]$^{2+}$ (bpy = 2,2′-bipyridine) to its *trans* form in water was first reported by Meyer[7] and later mechanistically characterized by Planas et al.[11] Recently, we reported the stoichiometric and irreversible photoisomerization of *d*-[Ru(tpy)(pynp)OH_2]$^{2+}$ (tpy = 2,2′:6′,2″-terpyridine and pynp = 2-(2-pyridyl)-1,8-naphthyridine) (*d*-**1H$_2$O**) to *p*-[Ru(tpy)-(pynp)OH_2]$^{2+}$ (*p*-**1H$_2$O**) (Scheme 1).[9] As a possible mechanism for the photoisomerization, we presumed, on the basis of previous reports,[4−6] that photodissociation of an aquo ligand on *d*-**1H$_2$O** could occur via a triplet metal-center transition (^{3}MC) state thermally accessible from the ^{3}MLCT

Scheme 1. Structures of Complexes[a]

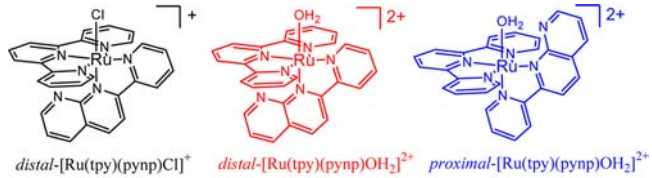

distal-[Ru(tpy)(pynp)Cl]$^+$ *d*-**1Cl**; *distal*-[Ru(tpy)(pynp)OH_2]$^{2+}$ *d*-**1H$_2$O**; *proximal*-[Ru(tpy)(pynp)OH_2]$^{2+}$ *p*-**1H$_2$O**

[a]The *d*-/*p*-isomers were defined by the structural configuration between the 1,8-naphthyridine moiety and the aquo or chloro ligand.

Received: January 8, 2013
Published: May 20, 2013

   dx.doi.org/10.1021/ic400054k | *Inorg. Chem.* 2013, 52, 6354−6364

photoexcited state, thereby forming a five-coordinate [Ru(tpy)(pynp)]$^{2+}$ intermediate. The *p*-**1H$_2$O** isomer would then be produced by recoordination of a water molecule to this intermediate from the opposite side relative to the tpy plane. However, information on the photoexcited state was limited and the mechanism for the photoisomerization was not further confirmed.

Polypyridyl ruthenium(II) aquo complexes are the subject of much recent attention relative to proton-coupled electron transfer[12,13] and water oxidation catalysis.[14−31] The stoichiometric character of the photoisomerization reaction of *d*-**1H$_2$O** enables efficient isolation of either the *d*- or *p*-**1H$_2$O** isomer, which makes it possible to compare the electron transfer reactions and water oxidation catalysis of both isomers. In a preliminary communication, we reported significant differences in these phenomena as a function of isomer, in addition to X-ray crystallographic structures for both isomers.[9] However, a rational explanation of these differences has not yet been advanced. Not long thereafter, Boyer et al. reported the catalysis for water oxidation by the *d*- and *p*-**1H$_2$O** isomer. They pointed out that the low turnover number of the *p*-**1H$_2$O** isomer might be due to catalyst decomposition, which was evident from carbon dioxide detected during catalysis run.[25] Clarifying those factors controlling redox properties and catalytic activities should prove useful in the design of improved molecular catalysts for water oxidation.

Quantum chemical calculations have proven to be useful in characterizing the mechanistic details of homogeneous transition-metal-based water oxidation catalysis,[16,22,24,31−50] particularly with respect to quantifying the energy barriers associated with alternative chemical steps potentially leading to O−O bond formation as part of the generation of molecular oxygen. Computation also offers microscopic insight into individual pK_a values, standard reduction potentials, and the nature of intermediates whose short lifetimes make them otherwise difficult to characterize. Especially when some experimental data are available against which to validate computational methodological choices, theory offers an opportunity to develop a rational basis for catalytic behavior and next-generation design efforts.

Herein we report theoretical investigations focusing on the mechanism of the stoichiometric and irreversible photoisomerization of *d*-**1H$_2$O** to *p*-**1H$_2$O**, as well as the redox and water-oxidation catalysis reactions for both isomers. We further report detailed experimental investigations including transient absorption spectra recorded on the nanosecond time scale. Data originally reported as Supporting Information for our earlier communication will be partially included in this work to facilitate our presentation.

EXPERIMENTAL AND THEORETICAL METHODS

Materials. 2-(2-Pyridyl)-1,8-naphthyridine (pynp)[51] and Ru(tpy)Cl$_3$[52] were prepared according to the literature. All other reagents were purchased and used without purification unless otherwise specified.

Synthesis and Characterization of Ruthenium Complexes. *1. distal-[Ru(tpy)(pynp)Cl]Cl (d-[**1Cl**]Cl).* *distal*-[Ru(tpy)(pynp)Cl]Cl was prepared referring to the previous method,[53] as follows. 101.8 mg (0.229 mmol) of Ru(tpy)Cl$_3$ and 43.2 mg (0.208 mmol) of pynp were refluxed for 4 h in 20 mL of 75 (v/v)% ethanol/water containing 52 mg (1.23 mmol) of LiCl and 1.45 mL (10.4 mmol) of triethylamine as a reductant in the dark. The reaction mixture was filtered hot, and the filtrate was concentrated to ∼4 mL with a rotary evaporator. The solution was then chilled in a refrigerator for 24 h. The solid was collected on a frit and washed with chilled 3 M HCl, acetone, and ether, and then dried in vacuo at room temperature to give *distal*-[Ru(tpy)(pynp)Cl]Cl (73.2 mg, 0.119 mmol, 57% yield). It was characterized by X-ray crystallographic analysis, ESI-MS, UV−visible, and NMR spectroscopic measurements. The structural conformation of *d*-**1Cl** was corroborated by ^{1}H−^{1}H COSY (correlation spectroscopy), ^{1}H−^{13}C HMQC (heteronuclear multiple-quantum correlation spectroscopy), and ^{1}H−^{13}C HMBC (heteronuclear multiple-bond correlation spectroscopy) measurements. UV−visible spectrum (H$_2$O): λ_{max} (ε) = 542 nm (8,600 M^{-1} cm^{-1}). MS(ESI): m/z^+ 577.21 (M). ^{1}H NMR (JEOL, 270 MHz, acetone-d_6): δ 10.61 (d, J = 4.9 Hz, 1H, $H_{6',pynp}$), 9.15 (d, J = 8.3 Hz, 1H, $H_{3',pynp}$), 8.79 (d, J = 8.7 Hz, 1H, $H_{3,pynp}$), 8.69 (d, J = 8.1 Hz, 2H, $H_{3',tpy}$), 8.49 (d, J = 8.2 Hz, 2H, $H_{3,tpy}$), 8.44 (dt, J = 8.1, 1.2 Hz, 1H, $H_{4',pynp}$), 8.41 (d, J = 8.7 Hz, 1H, $H_{4,pynp}$), 8.32 (d, J = 8.1 Hz, 1H, $H_{6,pynp}$), 8.26−8.17 (m, 2H, $H_{7,pynp}$, $H_{4',tpy}$), 8.11 (dt, J = 13.2 Hz, 1H, $H_{5',pynp}$), 7.86 (td, J = 8.2, 1.4 Hz, 2H, $H_{4,tpy}$), 7.71 (d, J = 4.9 Hz, 2H, $H_{6,tpy}$), 7.47 (dd, J = 8.2 and 4.3 Hz, 1H, $H_{6,pynp}$), and 7.25 (ddd, J = 8.2, 5.5, 1.2 Hz, 2H, $H_{5,tpy}$). ^{13}C NMR (JEOL, 67.8 MHz, acetone-d_6): δ 164.2 ($C_{2,pynp}$), 161.7 ($C_{2,tpy}$), 159.6 ($C_{10,pynp}$), 159.4 ($C_{2',tpy}$), 158.9 ($C_{2',pynp}$), 154.5 ($C_{6',pynp}$), 154.0 ($C_{7,pynp}$), 153.4 ($C_{6,tpy}$), 139.4 ($C_{5,pynp}$), 138.4 ($C_{4,pynp}$), 138.2 ($C_{4,tpy}$), 137.5 ($C_{4',pynp}$), 135.1 ($C_{4',tpy}$), 128.2 ($C_{5',pynp}$), 127.8 ($C_{5,tpy}$), 127.2 ($C_{3',pynp}$), 125.2 ($C_{6,pynp}$), 124.8 ($C_{9,pynp}$), 124.0 ($C_{3,tpy}$), 122.5 ($C_{3',tpy}$), 121.2 ($C_{3,pynp}$).

*2. distal-[Ru(tpy)(pynp)OH$_2$](PF$_6$)$_2$ (d-[**1H$_2$O**](PF$_6$)$_2$).* An aqueous solution of *d*-**1Cl** was left over 24 h in the dark to form *d*-**1H$_2$O** in solution. It was characterized by ESI-MS, UV−visible, and NMR spectroscopic measurements. The saturated NH_4PF_6 aqueous solution was added slowly to the solution, and then it was chilled in a refrigerator to give dark-purple crystalline *d*-[**1H$_2$O**](PF$_6$)$_2$. It was characterized by X-ray crystallographic analysis and elemental analysis. The structural conformation of *d*-**1H$_2$O** was corroborated by ^{1}H−^{1}H COSY, ^{1}H−^{13}C HMQC, and ^{1}H−^{13}C HMBC measurements. Anal. Calcd for $C_{28}H_{22}F_{12}N_6OP_2Ru{\cdot}2H_2O$: C, 37.98%; H, 2.96%; N, 9.49%. Found: C, 38.27%; H, 2.69%; N, 9.56%. UV−visible spectrum (H$_2$O): λ_{max} (ε) = 527 nm (9,300 M^{-1} cm^{-1}). MS(ESI): m/z^+ 559.11 (M − H). ^{1}H NMR (JEOL, 270 MHz, D$_2$O): δ 9.53 (d, J = 5.2 Hz, 1H, $H_{6',pynp}$), 8.76 (d, J = 8.6 Hz, 1H, $H_{3',pynp}$), 8.37 (d, J = 8.1 Hz, 2H, $H_{3',tpy}$), 8.30 (d, J = 8.6 Hz, 1H, $H_{3,pynp}$), 8.22 (t, J = 8.2 Hz, 1H, $H_{4',pynp}$), 8.16 (d, J = 8.2 Hz, 2H, $H_{3,tpy}$), 8.07 (t, J = 8.7 Hz, 1H, $H_{4',tpy}$), 8.02 (d, J = 8.8 Hz, 1H, $H_{4,pynp}$), 7.98 (d, J = 5.0 Hz, 1H, $H_{7,pynp}$), 7.95 (d, 8.0 Hz, 1H, $H_{5,pynp}$), 7.90 (m, 1H, $H_{5',pynp}$), 7.66 (t, J = 8.2 Hz, 2H, $H_{4,tpy}$), 7.52 (d, J = 5.4 Hz, 2H, $H_{6,tpy}$), 7.13 (dd, J = 8.0, 4.1 Hz, 1H, $H_{6,pynp}$), and 7.01 (t, J = 8.2 Hz, 2H, $H_{5,tpy}$). ^{13}C NMR (Varian, 176.0 MHz, D$_2$O): δ 162.9 ($C_{2,pynp}$), 160.0 ($C_{2,tpy}$), 158.4 ($C_{2',tpy}$), 157.9 ($C_{10,pynp}$), 157.1 ($C_{2',pynp}$), 152.8 ($C_{7,pynp}$), 152.6 ($C_{6,tpy}$), 150.3 ($C_{6',pynp}$), 137.9 ($C_{5,pynp}$), 137.6 ($C_{4,tpy}$), 137.3 ($C_{4,pynp}$), 136.5 ($C_{4',pynp}$), 135.2 ($C_{4',tpy}$), 127.2 ($C_{5',pynp}$), 126.7 ($C_{5,tpy}$), 125.9 ($C_{3',pynp}$), 123.5 ($C_{6,pynp}$), 123.0 ($C_{9,pynp}$), 122.9 ($C_{3,tpy}$), 121.6 ($C_{3',tpy}$), 119.5 ($C_{3,pynp}$).

*3. proximal-[Ru(tpy)(pynp)OH$_2$](PF$_6$)$_2$ (p-[**1H$_2$O**](PF$_6$)$_2$).* Visible light (λ > 420 nm) was irradiated to the *d*-**1H$_2$O** solution over 30 min from a filtered halogen lamp to form *p*-**1H$_2$O** in solution. It was characterized by ESI-MS, UV−visible, and NMR spectroscopic measurements. The saturated NH_4PF_6 aqueous solution was added slowly to the solution, and then it was chilled in a refrigerator to give dark-purple crystalline *p*-[**1H$_2$O**](PF$_6$)$_2$. The crystals were characterized by X-ray crystallographic analysis and elemental analysis. The structural conformation of *p*-**1H$_2$O** was corroborated by ^{1}H−^{1}H COSY, ^{1}H−^{13}C HMQC, and ^{1}H−^{13}C HMBC measurements. Anal. Calcd for $C_{28}H_{22}F_{12}N_6OP_2Ru{\cdot}0.5H_2O$: C, 39.17%; H, 2.70%; N, 9.84%. Found: C, 39.03%; H, 2.66%; N, 9.84%. UV−visible spectrum (H$_2$O): λ_{max} (ε) = 524 nm (9,300 M^{-1} cm^{-1}). MS(ESI): m/z^+ 559.31 (M − H). ^{1}H NMR (JEOL, 270 MHz, D$_2$O): δ 8.93 (dd, J = 4.5, 1.8 Hz, 1H, $H_{7,pynp}$), 8.82−8.67 (m, 3H, $H_{3,pynp}$, $H_{4,pynp}$, $H_{7,pynp}$), 8.44 (d, J = 8.2 Hz, 3H, $H_{3',pynp}$, $H_{3',tpy}$), 8.28 (d, J = 8.0 Hz, 2H, $H_{3,tpy}$), 8.12 (t, J = 8.2 Hz, 1H, $H_{4',tpy}$), 7.85 (dd, J = 8.3, 4.7 Hz, 1H, $H_{6,pynp}$), 7.75 (t, J = 8.2 Hz, 2H, $H_{4,tpy}$), 7.59 (t, J = 8.2 Hz, 1H, $H_{4',pynp}$), 7.46 (m, 3H, $H_{6',pynp}$, $H_{6,tpy}$), 7.00 (t, J = 6.5 Hz, 2H, $H_{5,tpy}$), and 6.89 (t, J = 6.5 Hz, 1H, $H_{5',pynp}$). ^{13}C NMR (Varian, 176.0 MHz, D$_2$O): δ 160.8 ($C_{2,pynp}$), 159.3 ($C_{2',pynp}$), 159.1 ($C_{2,tpy}$), 158.7 ($C_{2',tpy}$), 158.5 ($C_{10,pynp}$), 154.0

dx.doi.org/10.1021/ic400054k | Inorg. Chem. 2013, 52, 6354−6364

($C_{7,pynp}$), 153.8 ($C_{6,tpy}$), 153.3, 153.1 ($C_{6',pynp}$),, 141.2 ($C_{5,pynp}$), 139.1 ($C_{4,pynp}$), 138.9, 138.7 ($C_{4,tpy}$), 137.2 ($C_{4',tpy}$), 136.1, 135.9 ($C_{4',pynp}$), 127.9 ($C_{5,tpy}$), 127.2 ($C_{5',pynp}$), 126.6, 126.4 ($C_{3',pynp}$), 126.1 ($C_{9,pynp}$), 125.4, 125.3 ($C_{6,pynp}$), 124.7, 124.5 ($C_{3,tpy}$), 123.8, 123.5 ($C_{3',tpy}$ or $C_{3,pynp}$), 121.5 ($C_{3',tpy}$ or $C_{3,pynp}$).

Measurements. ^{1}H NMR spectra were recorded with a 270 MHz NMR spectrometer (JEOL) or a 700 MHz spectrometer (Varian) and calibrated using the solvent residual peak. UV visible absorption spectra were measured using a Shimadzu Multispec-1500 spectrophotometer. The ESI-MS spectra were collected on a mass spectrometer (Waters/Micromass, ZQ 4000) under the conditions employed (complex concentration, 5 μM; cone voltage, 20 V; capillary voltage, 3.5 kV). Nanosecond transient absorption spectra were acquired using a time-resolved spectrometer (Unisoku TSP-2000). The laser source was an optical parametric oscillator (OPO) (Continuum, Surelite) pumped by third harmonic of a Nd:YAG laser (Surelite I-10, pulse duration: 4 ns). The photodynamics was monitored by continuous exposure to a xenon lamp (150 W) or a halogen lamp as a probe light and a photomultiplier tube (Hamamatsu 2949) as a detector. Each sample solution was purged with Ar for at least 20 min prior to the measurement. Temperature of the solutions was controlled to ±0.1 °C with a circulating water bath. The cyclic voltammograms (CV) were measured in 0.5 mM Ru complex solutions (pH = 0.5−13.0) using a conventional single-compartment electrochemical cell equipped with a glassy carbon disk (3 mm diameter, 0.071 cm^2 effective area) or platinum mesh (ϕ = 0.07 cm, 0.8 × 1.0 cm) working electrode, a saturated calomel reference electrode (SCE), and a Pt wire counter electrode. The pHs of the electrolyte solutions were buffered at an ionic strength of 0.1 M by HNO_3 (pH 0−2), Na_2HPO_4 and KH_2PO_4 (pH 3−10), and NaOH (pH 11−14). The potential data (E_{SCE}/V) were converted to the potential (E_{NHE}/V) versus a normal hydrogen electrode (NHE) using $E_{NHE} = E_{SCE} + 0.238$ V. All the electrochemical experiments were implemented after bubbling argon gas for 20 min at 25 °C using an electrochemical analyzer (Hokuto Denko, HZ-3000). For chemical water oxidation experiments, an excess of Ce-$(NH_4)_2(NO_3)_6$ (0.5 mmol) as an oxidant was added quickly to a 20 μM *p*- or *d*-**1H$_2$O** aqueous solution (5.0 mL) in a gas-tight vessel under argon atmosphere at 25 °C and pH = 1.0. The pH change during the reaction for several hours was less than 0.1. The O_2 gas in the head space of the vessel was analyzed on a gas chromatograph (Shimadzu, GC-8A) equipped with a molecular sieve 5 Å column using argon carrier gas (flow rate = 40 cm^3 min^{-1}) at 50 °C and thermal conductivity detector.

COMPUTATIONAL METHODS

Density Functional Theory. All geometries were fully optimized at the M06-L level[54−56] of density functional theory using the Stuttgart [8s7p6d2f | 6s5p3d2f] ECP28MWB contracted pseudopotential basis set[57] on Ru and the 6-31G(d) basis set[58] on all other atoms. Nonanalytical integral evaluations made use of a pruned grid having 99 radial shells and 590 angular points per shell, and an automatically generated density-fitting basis set was used within the resolution-of-the-identity approximation to speed the evaluation of Coulomb integrals. The nature of all stationary points was verified by analytic computation of vibrational frequencies, which were also used for the computation of zero-point vibrational energies, molecular partition functions (with all frequencies below 50 cm^{-1} replaced by 50 cm^{-1} when computing free energies), and for determining the reactants and products associated with each transition-state structure (by following the normal modes associated with imaginary frequencies). Partition functions were used in the computation of 298 K thermal contributions to free energy employing the usual ideal-gas, rigid-rotator, harmonic oscillator approximation.[59] Free energy contributions were added to single-point M06-L electronic energies computed with the SDD basis set on ruthenium and the 6-311+G(2df,p) basis set on all other atoms to arrive at final, composite free energies for the water oxidation mechanism and added to M06[56] or M06-2X[56] electronic energies computed with the SDD basis set on ruthenium and the 6-311+G(d) basis set on all other atoms to arrive at final, composite free energies for the photoisomerization mechanism.

Solvation and Standard Reduction Potentials. Solvation effects associated with water as solvent were accounted for using the SMD continuum solvation model.[60] A 1 M standard state was used for all species in aqueous solution except for water itself, for which a 55.6 M standard state was employed. Thus, for all molecules but water, the free energy in aqueous solution is computed as the 1 atm gas-phase free energy, plus an adjustment for the 1 atm to 1 M standard-state concentration change of RT ln (24.5), or 1.9 kcal/mol, plus the 1 M to 1 M transfer (solvation) free energy computed from the SMD model. In the case of water, the 1 atm gas-phase free energy is adjusted by the sum of a 1 atm to 55.6 M standard-state concentration change, or 4.3 kcal/mol, and the experimental 1 M to 1 M solvation free energy, −6.3 kcal/mol. The 1 M to 1 M solvation free energy of the proton was taken from experiment as −265.9 kcal/mol.[61−64]

Standard reduction potentials were calculated for various possible redox couples to assess the energetic accessibility of different intermediates at various oxidation states. For a redox reaction of the form

$$O_{(aq)} + ne^-_{(g)} \rightarrow R_{(aq)} \quad (1)$$

where O and R denote the oxidized and reduced states of the redox couple, respectively, and n is the number of electrons involved in redox reaction, the reduction potential $E^o_{O|R}$ relative to NHE was computed as

$$E^o_{O|R} = -\frac{\Delta G^o_{O|R} - \Delta G^o_{NHE}}{nF} \quad (2)$$

where $\Delta G^o_{O|R}$ is the free energy change associated with eq 1 (using Boltzmann statistics for the electron), ΔG^0_{NHE} is the free energy change associated with

$$H^+_{(aq)} + e^-_{(g)} \rightarrow \frac{1}{2}H_{2(g)} \quad (3)$$

which is −4.28 eV with Boltzmann statistics for the electron,[63,65,66] and F is the Faraday constant.

Non-Single-Determinantal State Energies. Several possible intermediates in the water oxidation mechanism have electronic structures that are not well described by a single determinant. In such instances, standard Kohn−Sham DFT is not directly applicable,[59,67−69] and we adopt the Yamaguchi broken-spin-symmetry (BS) procedure[70,71] to compute the energy of the spin-purified low-spin (LS) state as

$${}^{LS}E = \frac{{}^{BS}E({}^{HS}\langle S^2\rangle - {}^{LS}\langle S^2\rangle) - {}^{HS}E({}^{BS}\langle S^2\rangle - {}^{LS}\langle S^2\rangle)}{{}^{HS}\langle S^2\rangle - {}^{BS}\langle S^2\rangle} \quad (4)$$

where HS refers to the single-determinantal high-spin coupled state that is related to the low-spin state by spin flip(s) and $\langle S^2\rangle$ is the expectation value of the total spin operator applied to the appropriate determinant. This broken-symmetry DFT approach has routinely proven effective for the prediction of state-energy splittings in metal coordination compounds.[68,72−75]

Time-Dependent Density Functional Theory (TDDFT) Calculations. TDDFT calculations were performed to predict the UV/visible electronic excitations of postulated intermediates. The M06[56] and M06-2X[56] density functionals, the Stuttgart [8s7p6d2f | 6s5p3d2f] ECP28MWB contracted pseudopotential basis set[57] on Ru, and the 6-311+G(d)[58] basis set on all other atoms were used for the TDDFT calculations. Nonequilibrium solvation effects were included via linear response approximation[76] in combination with the SMD aqueous continuum solvation model.[77] All calculations made use of the *Gaussian09* suite of electronic structure programs.[78]

RESULTS AND DISCUSSION

Synthesis of *d*-1Cl. *d*-[**1Cl**]Cl was synthesized by a reaction of Ru(tpy)Cl$_3$ and pynp according to the procedure provided by Thummel et al. Ru(tpy)Cl$_3$ and pynp were

dx.doi.org/10.1021/ic400054k | *Inorg. Chem.* 2013, 52, 6354−6364

refluxed in ethanol/water (3:1) containing LiCl and triethylamine for 4 h, and then the solvent was evaporated to dryness to give a deep purple solid residue. The ^{1}H NMR spectrum of the solid residue dissolved in $CDCl_3$ (Figure S1 in the Supporting Information) exhibited a doublet peak at 10.6 ppm assigned to a proton of *d*-**1Cl**, and all of the other main peaks were assigned to protons of *d*-**1Cl**, free tpy, and pynp. This corroborates that *d*-**1Cl** is predominantly formed as a main ruthenium species. Thummel et al. reported that the reaction of $Ru(tpy)Cl_3$ and pynp gave *d*-[**1Cl**](PF_6) (23% yield) and *p*-[**1H$_2$O**]$(PF_6)_2$ (24% yield) under nearly the same conditions. For their synthesis, *p*-[**1H$_2$O**]$(PF_6)_2$ can be formed by the aquation reaction of *d*-**1Cl** to *d*-**1H$_2$O** followed by photoisomerization of *d*-**1H$_2$O** to *p*-**1H$_2$O** during the purification process, both of which reactions will be discussed in below sections. This is consistent with the yield (57%) of *d*-[**1Cl**]Cl in the present synthesis that is close to the total yield of *d*-[**1Cl**](PF_6) (23% yield) and *p*-[**1H$_2$O**]$(PF_6)_2$ (24% yield).

In order to confirm influence of chloride anions on ligation of $Ru(tpy)Cl_3$ with pynp, the following synthetic experiment was carried out using silver nitrate as a halide abstraction agent. $Ru(tpy)Cl_3$, silver nitrate (3 equiv), and triethylamine were refluxed in EtOH/water for 2 h in the dark. To the resulting solution were added pynp with additional 4 h reflux, and the solvent was evaporated to dryness. The solid residue was partially dissolved in $CDCl_3$, and the ^{1}H NMR spectrum gave the peaks assigned to unreacted pynp (Figure S2A in the Supporting Information). The insoluble residue in $CDCl_3$ was dissolved in D_2O, and the ^{1}H NMR spectrum showed formation of *p*-**1H$_2$O** in contrast to selective formation of *d*-**1Cl** without a halide abstraction agent (Figure S2B in the Supporting Information). This result indicates that *p*-**1H$_2$O** is predominantly formed in the absence of chloride anions on the ligation reaction of $Ru(tpy)Cl_3$ with pynp. *d*-**1Cl** (not *proximal* isomer) could be selectively formed in the presence of chloride anions due to repulsion between the chloro ligand and a lone pair of the nitrogen atom of the naphthyridine moiety for the *proximal* isomer.

Aquation of *d*-1Cl to *d*-1H$_2$O. ^{1}H NMR spectrum of *d*-**1Cl** did not change for several days in the dark, showing that *d*-**1Cl** is stable in acetone-d_6. However, in the ^{1}H NMR spectrum of *d*-**1Cl** in D_2O the intensity of the peak observed at 10.0 ppm gradually decreased with time in the dark, concurrently with an increase of the doublet peak at 9.6 ppm assigned to the corresponding proton of *d*-**1H$_2$O** (Figure S3 in the Supporting Information). The peak intensity decreased according to first order kinetics with respect to the *d*-**1Cl** concentration.[9] This spectral change completed for 24 h at room temperature. The ^{1}H NMR data showed that *d*-**1Cl** stoichiometrically converts to *d*-**1H$_2$O** by exchange of a chloro ligand with solvent water in the dark.

In order to isolate *d*-**1H$_2$O** from the solution, solvent water was stripped to give a brown solid. The ^{1}H NMR spectrum (Figure S4 in the Supporting Information) of the solid redissolved in D_2O gave a peak at 10.0 ppm for *d*-**1Cl**, which gradually decreased with time, as observed in Figure S3 in the Supporting Information. This shows that an aquo ligand on *d*-**1H$_2$O** is exchanged by a chloro ion to recover *d*-**1Cl** stoichiometrically by stripping solvent. Nevertheless, *d*-**1H$_2$O** was successfully isolated by the addition of NH_4PF_6 to the solution of *d*-**1H$_2$O** and the crystals of *d*-[**1H$_2$O**]$(PF_6)_2$ salt were characterized by X-ray crystallographic analysis.[9]

The aquation reaction of *d*-**1Cl** was examined at various pH conditions (from 3.5 to 11) by ^{1}H NMR spectroscopy. The first order rate constant of the aquation reaction (k_{aq}/s^{-1}) did not change in this pH range ($k_{aq} = \sim 5.7 \times 10^{-5}$ s^{-1}) (Figure S5 in the Supporting Information). This result suggests that the aquation reaction of *d*-**1Cl** takes place in a dissociative or a dissociative interchange mechanism. Temperature dependence of k_{aq} was investigated; the k_{aq} value increased by a factor of 4.0 with a temperature increase from 288 to 313 K. Eyring plot for the aquation reaction gave a straight line (Figure S6 in the Supporting Information), and the activation parameters at 298 K were afforded as $\Delta H^{\ddagger} = 38.7$ kJ mol^{-1}, $\Delta S^{\ddagger} = -195$ J K^{-1} mol^{-1}, and $\Delta G^{\ddagger} = 97.1$ kJ mol^{-1}. These activation parameters are close to those ($\Delta H^{\ddagger} = 44.5$ kJ mol^{-1}, $\Delta S^{\ddagger} = -142$ J K^{-1} mol^{-1}) reported for the aquation reaction of *cis*-$[RuCl_2(cyclen)]^+$ complex[79] (cyclen = 1,4,7,10-tetraazacyclododecane).

Photoisomerization of *d*-1H$_2$O to *p*-1H$_2$O.[9] When visible light was irradiated to the aqueous solution of *d*-**1H$_2$O**, it was stoichiometrically photoisomerized to *p*-**1H$_2$O** (Figure S7 in the Supporting Information). The rate of the photoisomerization reaction is first order with respect to the *d*-**1H$_2$O** concentration. The internal quantum yield for photoisomerization is 1.5% (0.1 mM of *d*-**1H$_2$O** concentration). The rate constant (k_{pi}) of photoisomerization is constant in a range of pH 1−7 but decreases drastically at pH > 7, not occurring at pH > 11 (Figure S8 in the Supporting Information). This is corresponding to the absorbance change of the *d*-**1H$_2$O** solution in pH titration, showing that *d*-**1H$_2$O** (aquo form) is active for photoisomerization and that the deprotonation of an aquo ligand of *d*-**1H$_2$O** makes it inert for the photoisomerization. The photoisomerization is significantly temperature-controlled to give 41.7 ± 2.7 kJ/mol of activation energy at pH = 5.6. The activation energy (41.7 kJ/mol) is close but little smaller than the activation enthalpy (50.6−87.8 kJ/mol) for water exchange on ruthenium aquo complexes.[80−82]

Transient Absorption Spectroscopy of *d*-1H$_2$O and *p*-1H$_2$O. The UV−visible absorption spectrum of *d*-**1H$_2$O** gave a ^{3}MLCT absorption band at 526 nm which is very close to that of *p*-**1H$_2$O**, as shown in Figure S9 in the Supporting Information. This implies that the same photophysical and photochemical processes based on ^{3}MLCT are expected between these isomers when the visible light is irradiated to the solution of these isomers. The corresponding hydroxo complexes, *distal*- and *proximal*-$[Ru(tpy)(pynp)OH]^+$, are also expected to undergo the same processes because significant ^{3}MLCT absorption bands were given at 568 and 565 nm, respectively, although they shift to a low energy to a small extent. The ^{3}MLCT photoexcited states of these complexes were studied using a transient absorption spectroscopic technique to explore the mechanism of the photoisomerization. Transient absorption spectral change of the aqueous *d*-**1H$_2$O** solution after laser excitation (550 nm) at 275 K is shown in Figure 1. The spectral change is very similar to that observed for $[Ru(bpy)_3]^{2+}$.[83−85] The increase of the difference in optical density (ΔOD) at 390 nm and the bleach at 490 nm are assigned to generation of a ^{3}MLCT excited state and an extinction of the ground state of *d*-**1H$_2$O**, respectively. The intense bleaching at 830 nm can be assigned to the emission from the ^{3}MLCT state. The emission decay at 830 nm was analyzed by a single exponential curve fitting to give the observed first order rate constant, $k_{obs} = 1.1 \times 10^8$ s^{-1} (9 ns as

dx.doi.org/10.1021/ic400054k | Inorg. Chem. 2013, 52, 6354−6364

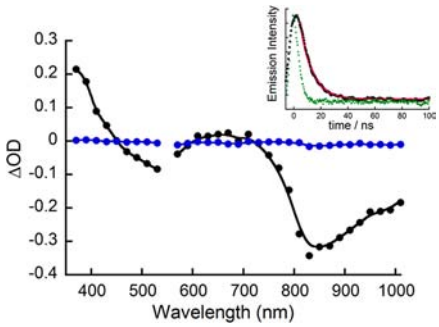

Figure 1. Transient absorption spectra of *d*-$\mathbf{1H_2O}$ (black) and *p*-$\mathbf{1H_2O}$ (blue) at 10 ns after excitation at 550 nm in water at 275 K under Ar atmosphere. Inset shows the emission decay (black) at 830 nm, simulated curve (red), and laser plus waveform (green).

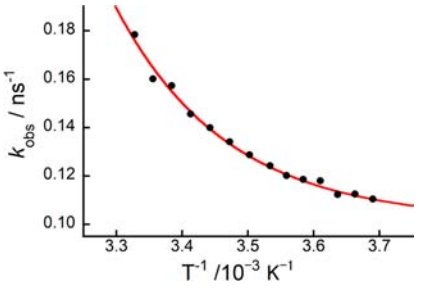

Figure 2. Temperature dependence of the observed rate constant (k_{obs}/s^{-1}) for decay of the ^{3}MLCT state of *d*-$\mathbf{1H_2O}$. The k_{obs} values were calculated from the emission decay at 830 nm. The solid line is a calculated line based on eq 5 by a least-squares fitting method.

lifetime of the ^{3}MLCT state) at 275 K as shown in the inset of Figure 1.

In contrast to the clearly observed spectral change for *d*-$\mathbf{1H_2O}$, no spectral change was observed for *p*-$\mathbf{1H_2O}$ under the same conditions, though the ^{3}MLCT state of *p*-$\mathbf{1H_2O}$ should be generated by 550 nm excitation, as the case of most polypyridyl ruthenium(II) complexes. This suggests that the lifetime (less than 1 ns at 275 K) of the ^{3}MLCT state of *p*-$\mathbf{1H_2O}$ is much shorter than that of *d*-$\mathbf{1H_2O}$. For the *distal*-hydroxo complex in an aqueous solution (pH = 11), no spectral change could be observed in our experimental set up at 275 K, suggesting that the lifetime of the photoexcited ^{3}MLCT state of *distal*-hydroxo complex is shorter than 1 ns at 275 K.

The transient absorption spectral measurement was carried out in a temperature range from 271 to 303 K for *d*-$\mathbf{1H_2O}$. The k_{obs} value increased from 1.1×10^8 s^{-1} to 1.6×10^8 s^{-1} with the temperature increase, and the temperature dependence of k_{obs} was analyzed by eq 5 considering thermal activated process:[86]

$$k_{obs} = k_d + k' \exp\left(-\frac{\Delta E}{RT}\right) \quad (5)$$

where k_d/s^{-1} is a first order rate constant for decay processes from the ^{3}MLCT state directly to the ground state including radiative (k_r/s^{-1}) and nonradiative (k_{nr}/s^{-1}) contributions ($k_d = k_r + k_{nr}$), and $k'\exp(-\Delta E/RT)$ is overall rate constants considering the thermally activated population. k'/s^{-1} is a pre-exponential factor of the thermally activated process with the activation energy (ΔE). The eq 5 was applied to the plots of k_{obs} versus $1/T$ using a nonlinear fitting method, and the best fitting was given at $k_d = 1.1 \pm 0.02 \times 10^8$ s^{-1}, $k' = 3.6 \pm 7.6 \times 10^{17}$ s^{-1}, and $\Delta E = 49 \pm 3$ kJ/mol (4100 cm^{-1}), as shown in Figure 2. The k_d and k' values mean that 38% of the ^{3}MLCT states is quenched through the thermally activated process at 298 K. It is most likely that the transition from the ^{3}MLCT state to the ^{3}MC state is responsible for the thermally activated process, because the ΔE value is close to the activation energy from the ^{3}MLCT state to the ^{3}MC state reported for a variety of polypyridyl ruthenium complexes.[87−90]

Theoretical Investigation on Photoisomerization of *d*-$\mathbf{1H_2O}$ to *p*-$\mathbf{1H_2O}$. Density functional theory (DFT) calculations at the M06 and M06-2X levels of theory were carried out in order to elucidate the mechanism of photoisomerization of *d*-$\mathbf{1H_2O}$ (see Computational Methods for details). Only M06 results will be presented here as the two levels of theory, which differ in the percentage of exact Hartree−Fock exchange that they include, agree to within 10.0 kJ/mol for all calculated energy changes. A comparison of M06 and M06-2X relative energies is available in the Supporting Information.

The proposed mechanism for the photoisomerization (Figure 3) starts with the photoexcitation of *d*-$\mathbf{1H_2O}$ (closed shell singlet, *d*-$\mathbf{S_0}$) to a first singlet excited state (*d*-$\mathbf{S_1}$). Intersystem crossing to a *d*-$\mathbf{T_1}$ state that is 33.0 kJ/mol lower in energy takes place next. Investigation of the molecular orbital changes associated with the generation of the *d*-$\mathbf{S_1}$ and *d*-$\mathbf{T_1}$ states from *d*-$\mathbf{S_0}$ indicates that the respective excitations can be characterized as metal to ligand charge transfer (^{3}MLCT) transitions (MOs in Figure 4, TD DFT data in Figure S10 in the Supporting Information). In the Franck−Condon *d*-$\mathbf{T_1}$ state, the interaction between the ruthenium center and the water molecule is found to be repulsive at all distances, so that the water molecule dissociates to form a pentacoordinated *d*-$\mathbf{T_{penta}}$ structure; the SOMOs of the *d*-$\mathbf{T_{penta}}$ structure are dominated by ruthenium d orbitals, indicating that, along the water dissociation coordinate, there is an electronic state crossing that takes place leading to the pentacoordinate ^{3}MC state (Figure 4). In solution, a low thermal activation energy to convert the vertical ^{3}MLCT structure (*d*-$\mathbf{T_1}$) to the ^{3}MC structure (*d*-$\mathbf{T_{penta}}$) is to be expected due to the solvent cage effect for the release of a bound H_2O molecule. An optimized structure for *distal*-[Ru(tpy)(pynp)OH]$^+$ with triplet spin state was also calculated, and it shows that the coordination of the hydroxyl ligand is sustained in contrast to the aquo case where the interaction between the ligand and ruthenium center is repulsive. We note that the rapid intersystem crossing and subsequent ^{3}MLCT → ^{3}MC state crossing outlined above is consistent with photophysical studies of analogous ruthenium complexes employing ultrafast X-ray spectroscopy.[91]

Two competing pathways are possible following the release of the water molecule from *d*-$\mathbf{T_1}$ and the generation of *d*-$\mathbf{T_{penta}}$. One pathway starts with the decay of *d*-$\mathbf{T_{penta}}$ to ground-state *d*-$\mathbf{S_{penta}}$, followed by a rate determining *d*-$\mathbf{S_{penta}}$ isomerization to *p*-$\mathbf{S_{penta}}$, and then coordination of a water molecule to *p*-$\mathbf{S_{penta}}$ in order to generate *p*-$\mathbf{1H_2O}$ (*p*-$\mathbf{S_0}$). The free energy of activation for the isomerization step (*d*-$\mathbf{S_{penta}}$ → *p*-$\mathbf{S_{penta}}$) is calculated to be 64.5 kJ/mol. An alternative pathway involves the pentacoordinate isomerization taking place on the triplet surface, i.e., *d*-$\mathbf{T_{penta}}$ to *p*-$\mathbf{T_{penta}}$, followed by decay to ground state *p*-$\mathbf{S_{penta}}$ and subsequent water coordination to generate again *p*-$\mathbf{1H_2O}$ (*p*-$\mathbf{S_0}$). Extensive efforts failed to locate a true transition-state structure for the isomerization step on the triplet surface (*d*-$\mathbf{T_{penta}}$ → *p*-$\mathbf{T_{penta}}$); however, constrained optimizations varying N−Ru−N angles to convert one isomer to another led to an approximate activation energy lower than

dx.doi.org/10.1021/ic400054k | Inorg. Chem. 2013, 52, 6354−6364

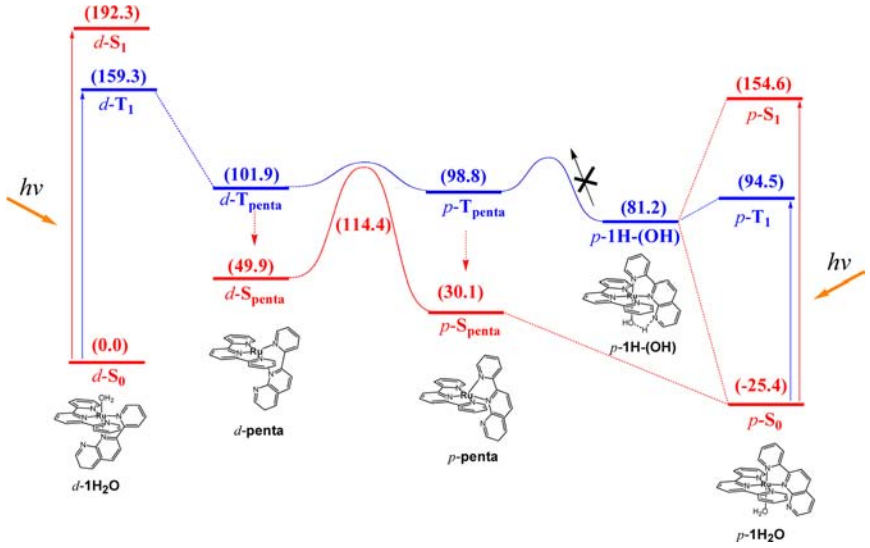

Figure 3. Energy diagram (M06//M06-L) for the photoisomerization process. Red curve denotes the singlet spin surface, and blue curve denotes the triplet spin surface. All energies are calculated on the basis of d-$\mathbf{S_0}$ and reported in units of kJ/mol.

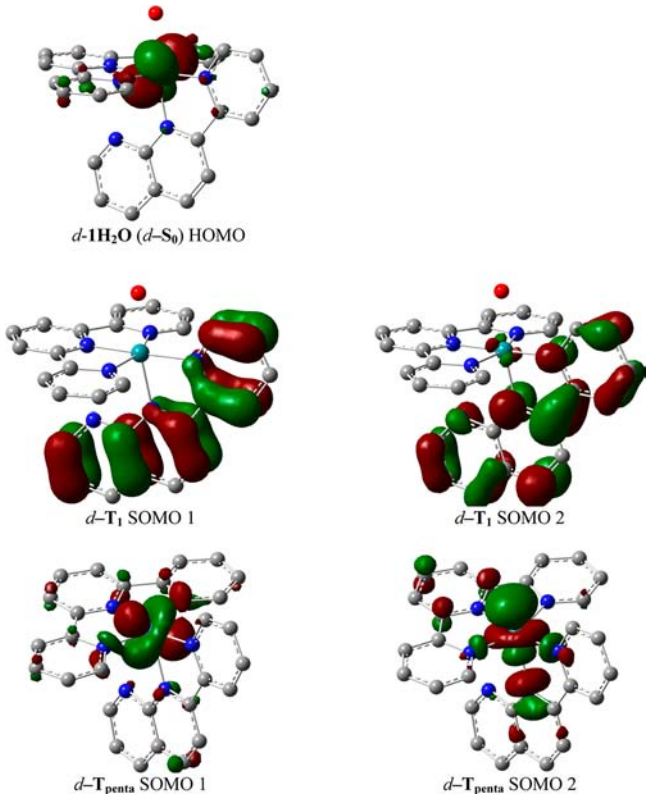

Figure 4. Molecular orbitals relevant to the isomerization mechanism of d-$\mathbf{1H_2O}$ (d-$\mathbf{S_0}$). Carbon atoms are gray, nitrogen atoms blue, oxygen atoms red, and Ru atoms cyan; hydrogen atoms are not shown for clarity.

that computed for the singlet surface. In each spin state, the *proximal* pentacoordinated structure is predicted to be lower in energy than the *distal* isomer. The actual path followed experimentally will depend on the relative rates of triplet decay and triplet isomerization, which we do not attempt to quantify here; indeed, it may be that isomerization proceeds competitively on both surfaces.

We have also investigated the possible photoisomerization of p-$\mathbf{1H_2O}$ and find that the photoexcitation of p-$\mathbf{1H_2O}$ (closed shell singlet, p-$\mathbf{S_0}$) can similarly access, through an intervening $\mathbf{S_1}$ state, a triplet excited-state structure having a bound H_2O molecule (named as p-$\mathbf{T_1}$). Interestingly, p-$\mathbf{T_1}$ is in equilibrium with the triplet excited-state of p-$\mathbf{1H\text{-}(OH)}$ which is 13.3 kJ/mol more stable and features a proton transfer from the aqua ligand to the pynp ligand so as to generate a structure having a hydroxo coordinated ruthenium center. In contrast to the triplet excited state of d-$\mathbf{1H_2O}$, the aquo and hydroxo ligands stay bound to the ruthenium center in p-$\mathbf{T_1}$ and p-$\mathbf{1H\text{-}(OH)}$, respectively, as they are stabilized by hydrogen bonding interactions. As a result, the photoexcited states decay directly to the ground state and back-isomerization to the *distal* form is predicted to be unfavorable.

Redox Reactions and Water Oxidation Catalysis of d-$\mathbf{1H_2O}$ and p-$\mathbf{1H_2O}$. The cyclic voltammograms (CV) of d- and p-$\mathbf{1H_2O}$ in an aqueous solution are shown in Figure 5. For d-$\mathbf{1H_2O}$, two redox waves were given at 0.68 and 0.84 V at pH = 7.0, assigned to $Ru^{II/III}$ and $Ru^{III/IV}$, respectively. These redox waves depended on pH of the electrolyte solution (Figure S11 in the Supporting Information). The half-wave potential ($E_{1/2}$) values d-$\mathbf{1H_2O}$ were pH-dependent in a wide range of pH = 1.5−10 (54 mV/pH for both the redox waves), being

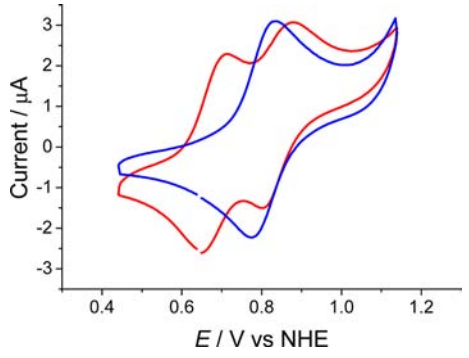

Figure 5. Cyclic voltammograms of 0.5 mM d-$\mathbf{1H_2O}$ (red) and p-$\mathbf{1H_2O}$ (blue) in 0.1 M phosphate buffer (pH 7). Scan rate: 50 mV s^{-1}. A grassy carbon electrode was used as a working electrode.

dx.doi.org/10.1021/ic400054k | Inorg. Chem. 2013, 52, 6354−6364

Table 1. Summary of $E_{1/2}$, pK_a, k_{O2}, and $\Delta G^{\ddagger}$ of *d*-$1H_2O$ and *p*-$1H_2O$[a]

	$E_{1/2}$/V vs NHE, pH 7.0		pK_a			
complexes	exptl	theor[b]	exptl	theor	k_{O2}[c]/10^{-4} s^{-1}	$\Delta G^{\ddagger}$[d]/kJ mol^{-1}
d-$1H_2O$	0.68, 0.84	0.27 (0.67), 0.52 (0.93)	9.7	10.8	38	87.9
p-$1H_2O$	0.81	0.52, 0.69	10.7	16.0	4.8	104.6

[a]Theory values at the M06-L level unless otherwise indicated. [b]M11-L theory values provided in parentheses. [c]k_{O2} values are experimental data. [d]$\Delta G^{\ddagger}$ values are M06-L theoretical calculations.

consistent with the earlier reported Pourbaix diagram of *d*-$1H_2O$.[9] This indicates that the two-step reaction of the 1-proton-coupled 1-electron reactions of $Ru^{II}-OH_2/Ru^{III}-OH$ and $Ru^{III}-OH/Ru^{IV}=O$ redox couples occurs for *d*-$1H_2O$ in the pH range. The electrochemical process is consistent with the previous reports on proton-coupled electron transfer (PCET) of ruthenium(II) aquo complexes.[17,92,93] The scan rate dependency of CV was examined, and the second wave became smaller and broader compared with the first one, as the scan rate increased (Figure S12 in the Supporting Information). This shows that the PCET in the second oxidation process is relatively slower than that in the first one, while only a redox wave was given at 0.81 V under the same conditions for *p*-$1H_2O$. The $E_{1/2}$ value of *p*-$1H_2O$ decreased with a pH increase in the range of pH = 1.5−10 (59 mV/pH), indicating that the one-step reaction of the 2-proton-coupled 2-electron reaction of the $Ru^{II}-OH_2/Ru^{IV}=O$ redox couple for *p*-$1H_2O$ at the pH range. This is also consistent with the earlier reported Pourbaix diagram of *p*-$1H_2O$.[9] Since the redox wave at 0.81 V for *p*-$1H_2O$ is relatively close to the second redox wave at 0.84 V, one may think the possibility that the isomerization of *d*-$1H_2O$ to *p*-$1H_2O$ is induced by the electrochemical oxidation. The CV data measured after the bulk electrolysis at 0.74 V (to form Ru^{III}) and 0.95 V (to form Ru^{IV}) and pH 7.0 were nearly identical to the CV before the bulk electrolysis (Figure S13 in the Supporting Information), excluding the possibility of the electrochemical isomerization of *d*-$1H_2O$.

For the CVs of *d*- and *p*-$1H_2O$ extended to 1.74 V (Figure S14 in the Supporting Information), the catalytic currents were exhibited above 1.44 V for both *d*- and *p*-$1H_2O$, assigned to water oxidation by detection of O_2 evolved on gas chromatograph. However, the current density (15.6 μA) at 1.74 V for *d*-$1H_2O$ is 2.2 times higher than that (7.1 μA) for *p*-$1H_2O$, showing that *d*-$1H_2O$ acts more effectively as a homogeneous catalyst for electrochemical water oxidation than *p*-$1H_2O$.

In order to reveal the catalytic activities of *d*- and *p*-$1H_2O$ isomers, chemical water oxidation experiments were conducted in a homogeneous aqueous solution using a Ce^{IV} oxidant. O_2 was evolved from the solution containing *d*- or *p*-$1H_2O$ and Ce^{IV}, and the turnover numbers of *d*-$1H_2O$ and *p*-$1H_2O$ were 62 and 2.4 at 12 h, showing that both isomers work as a catalyst. The initial O_2 evolution rates (v_{O2}/mol s^{-1}) increased linearly with the Ru amount (n_{Ru}/mol) for *d*- or *p*-$1H_2O$. This suggests that the O_2 evolution is a first order process with respect to *d*- or *p*-$1H_2O$.[9] The slope of the v_{O2} vs n_{Ru} plots for *d*-$1H_2O$ provides 3.8×10^{-3} s^{-1} of the turnover frequency (k_{O2}/s^{-1}), which is nearly the same as that (3.4×10^{-3} s^{-1})[9] of $[Ru(tpy)(bpy)OH_2]^{2+}$ with a similar structure under the same conditions. Nevertheless, it is higher than that (4.8×10^{-4} s^{-1}) for *p*-$1H_2O$ by nearly an order of magnitude. The CV data suggest that both the isomers are oxidized to $Ru^{IV}=O$ by reactions with Ce^{IV}. The $Ru^{IV}=O$ species could be further oxidized to $Ru^{V}=O$ for water oxidation. WNA on $Ru^{V}=O$ could be presumed to form an O−O bond during catalysis by both of the isomers. Boyer et al. reported the possibility of $Ru^{VI}=O$ species involved in water oxidation catalysis by the *d*- and *p*-$1H_2O$ isomers based on their electrochemical data.[25] However, it has to be pointed out that no spectroscopic evidence of $Ru^{VI}=O$ formation was provided. The experimental results from the current study are summarized in Table 1.

Theoretical Investigation on Proton-Coupled Electron Transfer and Water Oxidation Catalysis. DFT calculations at the M06-L level of theory using the SMD aqueous continuum solvation model offer mechanistic details for water oxidation proceeding via the *d*-$1H_2O$ or *p*-$1H_2O$ isomers (full cycles in Schemes 2 and 3 respectively with potentials reported

Scheme 2. Schematic Illustration for Water Oxidation by *d*-$1H_2O$ Based on DFT Calculation[a]

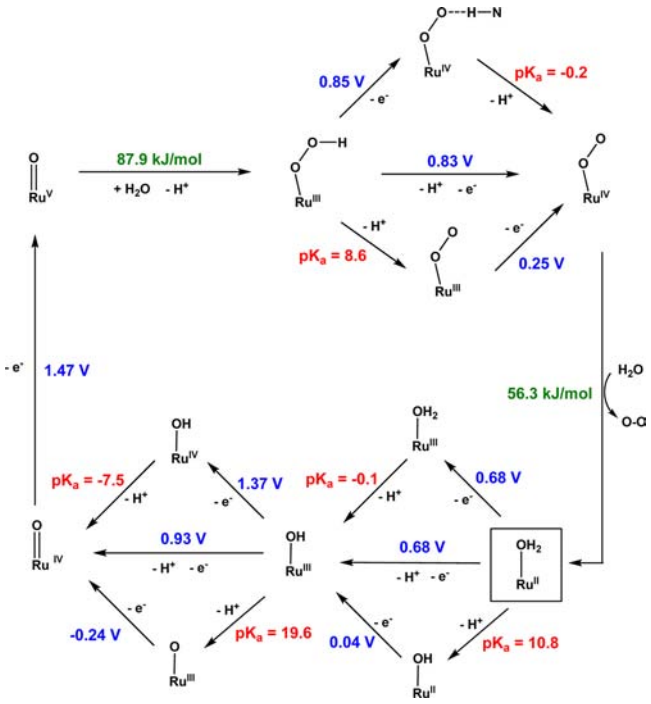

[a]All potentials are indicated versus NHE at pH = 0.

relative to NHE). Considering *d*-$[Ru^{II}-OH_2]^{2+}$, we found two consecutive PCET steps combine to generate *d*-$[Ru^{IV}-O]^{2+}$; the calculated redox potentials at pH = 7.0 (experimental pH conditions, which introduce a difference of 0.41 V with the NHE values reported in Scheme 2) are 0.27 and 0.52 V vs NHE, respectively, for the *d*-$[Ru^{III}-OH]^{2+}/$*d*-$[Ru^{II}-OH_2]^{2+}$ and *d*-$[Ru^{IV}-O]^{2+}/$*d*-$[Ru^{III}-OH]^{2+}$ couples. The experimentally observed values are 0.68 and 0.84 V vs NHE, respectively. DFT calculations involving continuum solvation models have been shown often to be accurate to within 100 mV for reduction potentials, and we and others have had good success

dx.doi.org/10.1021/ic400054k | Inorg. Chem. 2013, 52, 6354−6364

Scheme 3. Schematic Illustration for Water Oxidation by *p*-1H$_2$O Based on DFT Calculation[a]

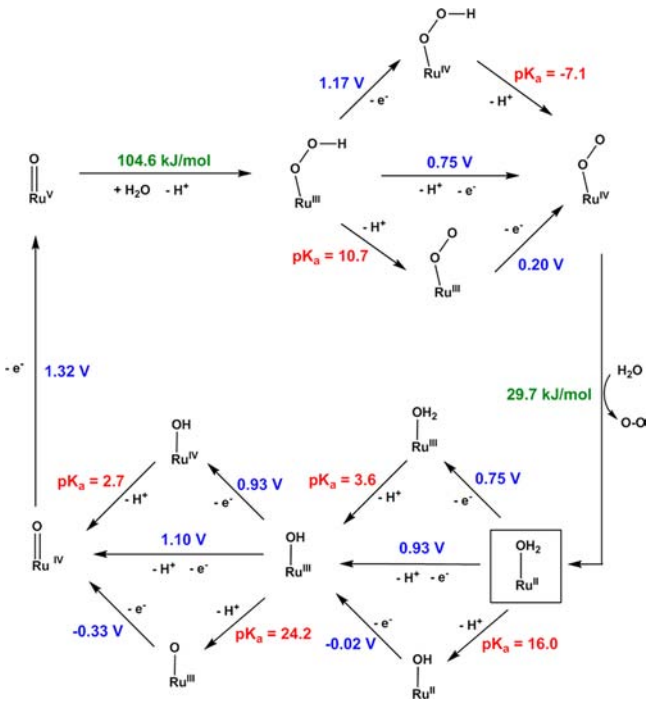

[a]All potentials are indicated versus NHE at pH = 0.

in prior studies of transition metal containing systems.[65,66,94−105] The prediction of pK_a values using continuum solvation approaches has also been studied extensively,[66,94−108] and based on experience we estimate a conservative (i.e., worst case) error for this process of about 300 mV (or about 5 pK units). As PCET free energy changes implicitly include both electron and proton transfer steps (the proton and electron transfers involved in these PCET steps are expected to proceed at diffusion controlled rates), a worst-case error estimate is on the order of 400 mV. Our calculations in this study display deviations from the experimental values on the order of this error estimate, which prompted us to look more closely at the likely source of the largest error. We further investigated the first two PCET steps for *d*-**1H$_2$O** and found that the calculated potentials depend significantly on the choice of functional and basis set. For example, the calculated potentials vs NHE at pH 7.0 with the more recently reported M11-L functional[109] are 0.67 and 0.93 V, respectively, for the first two PCET steps for *d*-**1H$_2$O**, which is in near quantitative agreement with the experimentally observed values (Table 1; it is a coincidence that the difference between the M06-L and M11-L predictions is almost exactly equal to the 0.41 V correction for adjusting the NHE standard state potential from pH = 0 to pH = 7). Based on these results, we have also examined other steps in the proposed mechanisms with the M11-L functional and found negligible differences (less than 4 kJ/mol in investigated steps) in free energy changes and free energy of activation values. We have also investigated the effect of inclusion of explicit first shell water molecules, and found only marginal improvement in the calculated redox potentials. These observations will merit attention in future studies of metal-catalyzed water oxidation reactions, but we will not explore the PCET details more closely here, and we continue to discuss the mechanism in terms of our original M06-L calculations.

In terms of electronic structure, *d*-[**Ru^{II}−OH$_2$**]$^{2+}$ has a closed-shell singlet ground state, *d*-[**Ru^{III}−OH**]$^{2+}$ has a doublet ground state, and *d*-[**Ru^{IV}−O**]$^{2+}$ has a triplet ground state. As a formal Ru^{IV}═O species, the oxo group in *d*-[**Ru^{IV}−O**]$^{2+}$ could in principle be susceptible to nucleophilic attack by a water molecule. However, our attempts to locate a transition-state (TS) structure for this process were unsuccessful even in the presence of additional explicit water molecules which might assist in proton translocation from the nucleophilic water molecule as part of O−O bond formation.

Following this observation, we considered possible additional oxidation of *d*-[**Ru^{IV}−O**]$^{2+}$ to *d*-[**Ru^{V}−O**]$^{3+}$, which was found to have a calculated oxidation potential of 1.47 V at the M06-L level of theory. Water nucleophilic attack (WNA) on the *d*-[**Ru^{V}−O**]$^{3+}$ structure, which has a doublet electronic ground state, was found to proceed through a pentamolecular transition-state structure (also having a doublet ground state), which combines proton transfer from the attacking water to an adjacent first shell water molecule with concomitant O−O bond formation (Figure 6). The free energy of activation for

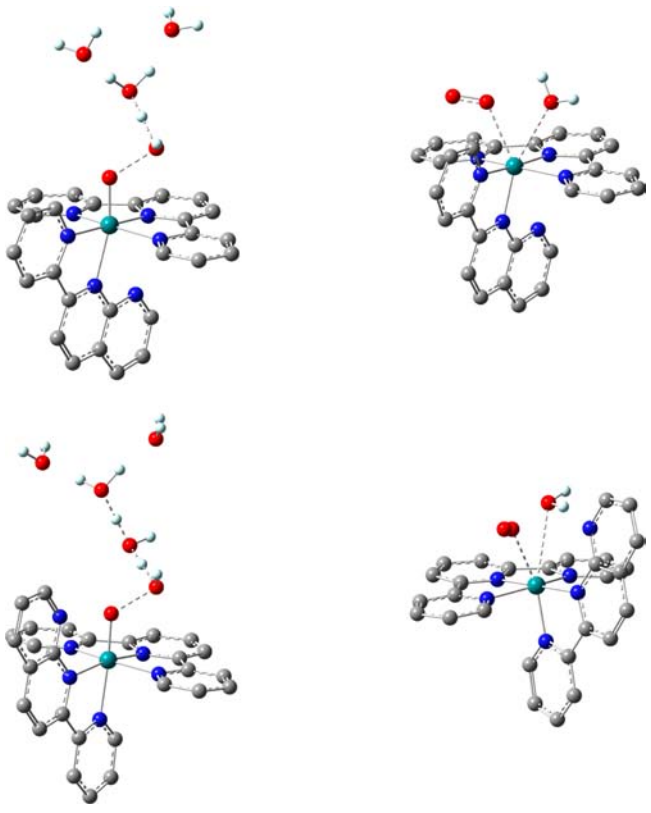

Figure 6. M06-L transition-state structures for O−O bond formation O_2 liberation for *d*-**1H$_2$O** (top) and *p*-**1H$_2$O** (bottom) catalysts. Carbon atoms are gray, nitrogen atoms blue, oxygen atoms red, and Ru atoms cyan; ligand hydrogen atoms are not shown for clarity.

this step is predicted to be 87.9 kJ/mol (Scheme 2, Table 1), and the resulting product is a doublet hydroperoxo intermediate, *d*-[**Ru^{III}−OOH**]$^{2+}$. A following PCET, either stepwise or concerted, leads to formation of open-shell singlet *d*-[**Ru^{IV}−OO**]$^{2+}$ which releases O_2 upon a water displacement reaction at the ruthenium center thereby regenerating the initial catalyst *d*-[**Ru^{II}−OH$_2$**]$^{2+}$. This final step is predicted to have a free energy of activation of 56.3 kJ/mol (Scheme 2).

dx.doi.org/10.1021/ic400054k | *Inorg. Chem.* 2013, 52, 6354−6364

An analogous water oxidation mechanism is also predicted for *p*-**1H$_2$O** with two distinctions (Scheme 3). First, from the experimental data *p*-[**Ru^{II}−OH$_2$**]$^{2+}$ exhibits only a single redox wave at 0.81 V assigned to a two-electron *p*-[**Ru^{IV}−O**]$^{2+}$/*p*-[**Ru^{II}−OH$_2$**]$^{2+}$ couple. The average oxidation potential for these two steps is calculated to be 0.61 V at the M06-L level of theory (the two individual potentials are predicted computationally to differ by 0.17 V) (Scheme 3, Table 1). Second, we found the WNA transition state for *p*-[**Ru^{V}−O**]$^{3+}$ to require a hexamolecular structure and to proceed with a free energy of activation of 104.6 kJ/mol (Scheme 3, Table 1). Our attempts to locate a pentamolecular TS structure for WNA on *p*-[**Ru^{V}−O**]$^{3+}$ were unsuccessful. We were able to locate a similar hexamolecular TS structure for *d*-[**Ru^{V}−O**]$^{3+}$ as well, which features a $\Delta G^{\ddagger}$ of 92.7 kJ/mol (Figure 6) (see Supporting Information). The decisive influence of first-solvent shell water on computed WNA transition-state structures has been noted previously.[35,37,40,43,49]

Significance. *Mechanism of Photoisomerization of d-1H$_2$O to p-1H$_2$O.* As for the mechanism of photoisomerization, the thermally activated process from the ^{3}MLCT state to the ^{3}MC state which was evident from nanosecond transient absorption spectroscopic measurement might be a main activation process because the activation energy (ΔE = 49 kJ mol^{-1}) is close to that (41.7 kJ mol^{-1}) of the overall photoisomerization reaction. However, DFT calculations suggested another activation process for the conformation change of the pentacoordinated *distal*-structure to the *proximal*-structure, the latter of which is lower in energy than the former in the singlet and triplet spin states. We suggest that the triplet excited state of *p*-**1H$_2$O** is lower in energy than that of *d*-**1H$_2$O** due to hydrogen bonding between an aquo ligand and a naphthyridine moiety of the pynp ligand. This is consistent with the shorter lifetime (less than 1 ns at 275 K) of the triplet excited state of *p*-**1H$_2$O** than that (9 ns at 275 K) of *d*-**1H$_2$O**. The DFT calculations also suggest that dissociation of the aquo ligand is disfavored by the hydrogen bond. The shorter lifetime of the triplet excited state of *p*-**1H$_2$O** and the disfavored aquo ligand dissociation could be responsible for the irreversible photoisomerization. The key role of the hydrogen bond interaction for photoisomerization will come to be more clear if experimental and theoretical investigations on the photoisomerization reaction of ruthenium complex derivatives with a 2-(2-pyridyl)quinoline ligand instead of the pynp ligand are conducted.

Mechanism of Water Oxidation Catalysis. The proposed water oxidation mechanisms for both *d*-[**Ru^{II}−OH$_2$**]$^{2+}$ and *p*-[**Ru^{II}−OH$_2$**]$^{2+}$ indicate that WNA on the [**Ru^{V}−O**]$^{3+}$ group is the rate determining step in the presence of excess sacrificial oxidant and WNA for *d*-[**Ru^{V}−O**]$^{3+}$ is favored over *p*-[**Ru^{V}−O**]$^{3+}$. Examination of the lowest unoccupied molecular orbitals (LUMO) in these two formal oxo species indicates that more orbital amplitude is concentrated on the [Ru−O] unit in the case of *d*-[**Ru^{V}−O**]$^{3+}$ than in the case of *p*-[**Ru^{V}−O**]$^{3+}$, where some of the amplitude is instead delocalized over the pynp ligand (Figure 7). Since these are the acceptor orbitals for the WNA step, orbital amplitude concentrated on the [Ru−O] unit improves overlap with the nucleophilic water lone pair orbital and renders more favorable the formation of an O−O bond in the WNA step than is the case when the orbital amplitude is reduced on the [Ru−O] unit through delocalization over the pynp ligand. This rationalizes the lower free energy of activation for the [**Ru^{V}−O**]$^{3+}$ unit in the *distal* isomer compared to the *proximal* one. The LUMO amplitude localized on the heterocycle is also consistent with the low turnover number of the *proximal* isomer which was attributed to ligand decomposition based on carbon dioxide detected during catalysis, as reported in the earlier study.[25] The oxidative decomposition of *p*-**1H$_2$O** might be caused by the WNA to the orbital amplitude delocalized over the pynp ligand on *p*-[**Ru^{V}−O**]$^{3+}$ although the full mechanism of decomposition is still unclear.

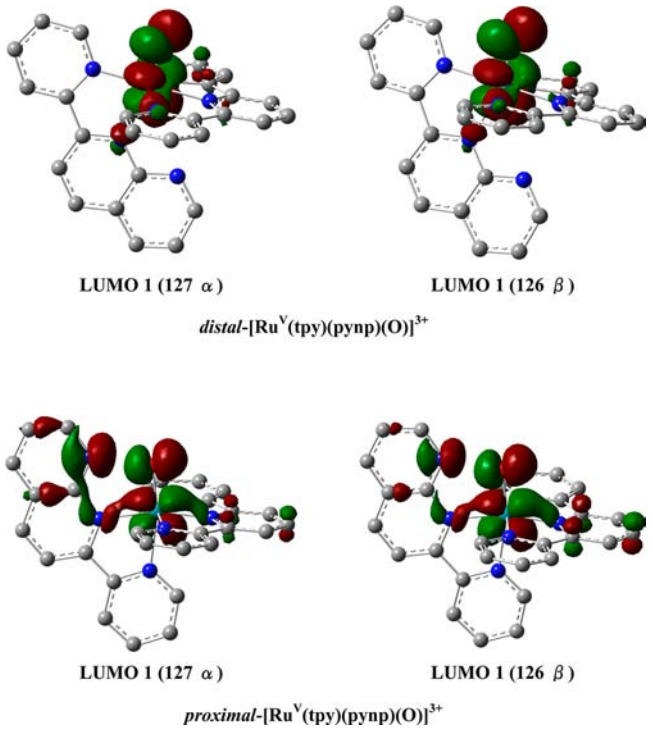

Figure 7. Molecular orbitals of the lowest unoccupied molecular orbitals (LUMO) of *d*-Ru^{V}=O (top) and *p*-Ru^{V}=O (bottom). Carbon atoms are gray, nitrogen atoms blue, oxygen atoms red, and Ru atoms cyan; hydrogen atoms are not shown for clarity.

■ ASSOCIATED CONTENT

Ⓢ Supporting Information

Additional experimental data including ^{1}H NMR spectra, plots of rate constant vs pH, Eyring plot, UV−vis spectra, tables of relative energies and redox potentials, cyclic voltammograms, and Cartesian coordinates and energies. This material is available free of charge via the Internet at http://pubs.acs.org.

■ AUTHOR INFORMATION

Corresponding Author

*E-mail: yagi@eng.niigata-u.ac.jp. Fax: +81-25-262-6790.

Notes

The authors declare no competing financial interest.

■ ACKNOWLEDGMENTS

Financial support from JST PRESTO program, Grant-in-Aid for Scientific Research (B) from the Ministry of Education, Culture, Sports, Science and Technology (No. 24350028), the U.S. National Science Foundation (CHE-0952054) and the Graduate School of the University of Minnesota (doctoral dissertation fellowship for M.Z.E.) is gratefully acknowledged.

REFERENCES

(1) Kalyanasundaram, K. *Coord. Chem. Rev.* **1982**, *46*, 159.
(2) Balzani, V.; Juris, A. *Coord. Chem. Rev.* **2001**, *211*, 97.
(3) Juris, A.; Balzani, V.; Barigelletti, F.; Campagna, S.; Belser, P.; Vonzelewsky, A. *Coord. Chem. Rev.* **1988**, *84*, 85.
(4) Pinnick, D. V.; Durham, B. *Inorg. Chem.* **1984**, *23*, 1440.
(5) Durham, B.; Walsh, J. L.; Carter, C. L.; Meyer, T. J. *Inorg. Chem.* **1980**, *19*, 860.
(6) Hecker, C. R.; Fanwick, P. E.; McMillin, D. R. *Inorg. Chem.* **1991**, *30*, 659.
(7) Durham, B.; Wilson, S. R.; Hodgson, D. J.; Meyer, T. J. *J. Am. Chem. Soc.* **1980**, *102*, 600.
(8) Porter, G. B.; Sparks, R. H. *J. Photochem.* **1980**, *13*, 123.
(9) Yamazaki, H.; Hakamata, T.; Komi, M.; Yagi, M. *J. Am. Chem. Soc.* **2011**, *133*, 8846.
(10) Padhi, S. K.; Fukuda, R.; Ehara, M.; Tanaka, K. *Inorg. Chem.* **2012**, *51*, 5386.
(11) Planas, N.; Vigara, L.; Cady, C.; Miro, P.; Huang, P.; Hammarstrom, L.; Styring, S.; Leidel, N.; Dau, H.; Haumann, M.; Gagliardi, L.; Cramer, C. J.; Llobet, A. *Inorg. Chem.* **2011**, *50*, 11134.
(12) Huynh, M. H. V.; Meyer, T. J. *Chem. Rev.* **2007**, *107*, 5004.
(13) Mayer, J.; Rhile, I.; Larsen, F.; Mader, E.; Markle, T.; Dipasquale, A. *Photosynth. Res.* **2006**, *87*, 21.
(14) Gersten, S. W.; Samuels, G. J.; Meyer, T. J. *J. Am. Chem. Soc.* **1982**, *104*, 4029.
(15) Concepcion, J. J.; Jurss, J. W.; Templeton, J. L.; Meyer, T. J. *J. Am. Chem. Soc.* **2008**, *130*, 16462.
(16) Concepcion, J. J.; Tsai, M.-K.; Muckerman, J. T.; Meyer, T. J. *J. Am. Chem. Soc.* **2010**, *132*, 1545.
(17) Concepcion, J. J.; Jurss, J. W.; Norris, M. R.; Chen, Z. F.; Templeton, J. L.; Meyer, T. J. *Inorg. Chem.* **2010**, *49*, 1277.
(18) Pramanik, N. C.; Bhattacharya, S. *Transition Met. Chem. (London)* **1997**, *22*, 524.
(19) Wada, T.; Tsuge, K.; Tanaka, K. *Angew. Chem., Int. Ed.* **2000**, *39*, 1479.
(20) Sens, C.; Romero, I.; Rodriguez, M.; Llobet, A.; Parella, T.; Benet-Buchholz, J. *J. Am. Chem. Soc.* **2004**, *126*, 7798.
(21) Masllorens, E.; Rodriguez, M.; Romero, I.; Roglans, A.; Parella, T.; Benet-Buchholz, J.; Poyatos, M.; Llobet, A. *J. Am. Chem. Soc.* **2006**, *128*, 5306.
(22) Sala, X.; Ertem, M. Z.; Vigara, L.; Todorova, T. K.; Chen, W.; Rocha, R. C.; Aquilante, F.; Cramer, C. J.; Gagliardi, L.; Llobet, A. *Angew. Chem., Int. Ed.* **2010**, *49*, 7745.
(23) Zong, R.; Thummel, R. P. *J. Am. Chem. Soc.* **2005**, *127*, 12802.
(24) Polyansky, D. E.; Muckerman, J. T.; Rochford, J.; Zong, R. F.; Thummel, R. P.; Fujita, E. *J. Am. Chem. Soc.* **2011**, *133*, 14649.
(25) Boyer, J. L.; Polyansky, D. E.; Szalda, D. J.; Zong, R.; Thummel, R. P.; Fujita, E. *Angew. Chem., Int. Ed.* **2011**, *50*, 12600.
(26) Yagi, M.; Syouji, A.; Yamada, S.; Komi, M.; Yamazaki, H.; Tajima, S. *Photochem. Photobiol. Sci.* **2009**, *8*, 139.
(27) Yagi, M.; Tajima, S.; Komi, M.; Yamazaki, H. *Dalton Trans.* **2011**, *40*, 3802.
(28) Masaoka, S.; Sakai, K. *Chem. Lett.* **2009**, *38*, 182.
(29) Xu, Y.; Fischer, A.; Duan, L.; Tong, L.; Gabrielsson, E.; Åkermark, B.; Sun, L. *Angew. Chem., Int. Ed.* **2010**, *49*, 8934.
(30) Duan, L.; Bozoglian, F.; Mandal, S.; Stewart, B.; Privalov, T.; Llobet, A.; Sun, L. *Nat. Chem.* **2012**, *4*, 418.
(31) Wasylenko, D. J.; Ganesamoorthy, C.; Koivisto, B. D.; Henderson, M. A.; Berlinguette, C. P. *Inorg. Chem.* **2010**, *49*, 2202.
(32) Yang, X.; Baik, M. H. *J. Am. Chem. Soc.* **2006**, *128*, 7476.
(33) Muckerman, J. T.; Polyansky, D. E.; Wada, T.; Tanaka, K.; Fujita, E. *Inorg. Chem.* **2008**, *47*, 1787.
(34) Yang, X. F.; Baik, M. H. *J. Am. Chem. Soc.* **2008**, *130*, 16231.
(35) Bozoglian, F.; Romain, S.; Ertem, M. Z.; Todorova, T. K.; Sens, C.; Mola, J.; Rodriguez, M.; Romero, I.; Benet-Buchholz, J.; Fontrodona, X.; Cramer, C. J.; Gagliardi, L.; Llobet, A. *J. Am. Chem. Soc.* **2009**, *131*, 15176.
(36) Hull, J. F.; Balcells, D.; Blakemore, J. D.; Incarvito, C. D.; Eisenstein, O.; Brudvig, G. W.; Crabtree, R. H. *J. Am. Chem. Soc.* **2009**, *131*, 8730.
(37) Wang, L. P.; Wu, Q.; Van Voorhis, T. *Inorg. Chem.* **2010**, *49*, 4543.
(38) Blakemore, J. D.; Schley, N. D.; Balcells, D.; Hull, J. F.; Olack, G. W.; Incarvito, C. D.; Eisenstein, O.; Brudvig, G. W.; Crabtree, R. H. *J. Am. Chem. Soc.* **2010**, *132*, 16017.
(39) Kuznetsov, A. E.; Geletii, Y. V.; Hill, C. L.; Musaev, D. G. *J. Phys. Chem. A* **2010**, *114*, 11417.
(40) Bianco, R.; Hay, P. J.; Hynes, J. T. *J. Phys. Chem. A* **2011**, *115*, 8003.
(41) Vilella, L.; Vidossich, P.; Balcells, D.; Lledos, A. *Dalton Trans.* **2011**, *40*, 11241.
(42) Wang, L. P.; Van Voorhis, T. *J. Phys. Chem. Lett.* **2011**, *2*, 2200.
(43) Li, X. C.; Chen, G. J.; Schinzel, S.; Siegbahn, P. E. M. *Dalton Trans.* **2011**, *40*, 11296.
(44) Radaram, B.; Ivie, J. A.; Singh, W. M.; Grudzien, R. M.; Reibenspies, J. H.; Webster, C. E.; Zhao, X. *Inorg. Chem.* **2011**, *50*, 10564.
(45) Busch, M.; Ahlberg, E.; Panas, I. *Phys. Chem. Chem. Phys.* **2011**, *13*, 15069.
(46) Hughes, T. F.; Friesner, R. A. *J. Phys. Chem. B* **2011**, *115*, 9280.
(47) Ghosh, S.; Baik, M. H. *Inorg. Chem.* **2011**, *50*, 5946.
(48) Valles-Pardo, J. L.; Guijt, M. C.; Iannuzzi, M.; Joya, K. S.; de Groot, H. J. M.; Buda, F. *ChemPhysChem* **2012**, *13*, 140.
(49) Ertem, M. Z.; Gagliardi, L.; Cramer, C. J. *Chem. Sci.* **2012**, *3*, 1293.
(50) Vigara, L.; Ertem, M. Z.; Planas, N.; Bozoglian, F.; Leidel, N.; Dau, H.; Haumann, M.; Gagliardi, L.; Cramer, C. J.; Llobet, A. *Chem. Sci.* **2012**, *3*, 2576.
(51) Tseng, H.-W.; Zong, R.; Muckerman, J. T.; Thummel, R. *Inorg. Chem.* **2008**, *47*, 11763.
(52) Sullivan, B. P.; Calvert, J. M.; Meyer, T. J. *Inorg. Chem.* **1980**, *19*, 1404.
(53) Campos-Fernández, C. S.; Thomson, L. M.; Galán-Mascarós, J. R.; Ouyang, X.; Dunbar, K. R. *Inorg. Chem.* **2002**, *41*, 1523.
(54) Zhao, Y.; Truhlar, D. G. *J. Chem. Phys.* **2006**, *125*, 194101.
(55) Zhao, Y.; Truhlar, D. G. *Acc. Chem. Res.* **2008**, *41*, 157.
(56) Zhao, Y.; Truhlar, D. G. *Theor. Chem. Acc.* **2008**, *120*, 215.
(57) Andrae, D.; Haussermann, U.; Dolg, M.; Stoll, H.; Preuss, H. *Theor. Chim. Acta* **1990**, *77*, 123.
(58) Hehre, W. J.; Radom, L.; Schleyer, P. v. R.; Pople, J. A. *Ab Initio Molecular Orbital Theory*; Wiley: New York, 1986.
(59) Cramer, C. J. *Essentials of Computational Chemistry: Theories and Models*, 2nd ed.; John Wiley & Sons: Chichester, 2004.
(60) Marenich, A. V.; Cramer, C. J.; Truhlar, D. G. *J. Phys. Chem. B* **2009**, *113*, 6378.
(61) Tissandier, M. D.; Cowen, K. A.; Feng, W. Y.; Gundlach, E.; Cohen, M. H.; Earhart, A. D.; Coe, J. V.; Tuttle, T. R. *J. Phys. Chem. A* **1998**, *102*, 7787.
(62) Camaioni, D. M.; Schwerdtfeger, C. A. *J. Phys. Chem. A* **2005**, *109*, 10795.
(63) Kelly, C. P.; Cramer, C. J.; Truhlar, D. G. *J. Phys. Chem. B* **2006**, *110*, 16066.
(64) Bryantsev, V. S.; Diallo, M. S.; Goddard, W. A. *J. Phys. Chem. B* **2008**, *112*, 9709.
(65) Lewis, A.; Bumpus, J. A.; Truhlar, D. G.; Cramer, C. J. *J. Chem. Educ.* **2004**, *81*, 596.
(66) Winget, P.; Cramer, C. J.; Truhlar, D. G. *Theor. Chem. Acc.* **2004**, *112*, 217.
(67) Ziegler, T.; Rauk, A.; Baerends, E. J. *Theor. Chim. Acta* **1977**, *43*, 261.
(68) Noodleman, L. *J. Chem. Phys.* **1981**, *74*, 5737.
(69) Cramer, C. J.; Truhlar, D. G. *Phys. Chem. Chem. Phys.* **2009**, *11*, 10757.
(70) Yamaguchi, K.; Jensen, F.; Dorigo, A.; Houk, K. N. *Chem. Phys. Lett.* **1988**, *149*, 537.

(71) Soda, T.; Kitagawa, Y.; Onishi, T.; Takano, Y.; Shigeta, Y.; Nagao, H.; Yoshioka, Y.; Yamaguchi, K. *Chem. Phys. Lett.* **2000**, *319*, 223.
(72) Noodleman, L.; Peng, C. Y.; Case, D. A.; Mouesca, J.-M. *Coord. Chem. Rev.* **1995**, *144*, 199.
(73) Ciofini, I.; Daul, C. A. *Coord. Chem. Rev.* **2003**, *238*, 187.
(74) Harvey, J. N. *Struct. Bonding (Berlin)* **2004**, *112*, 151.
(75) Neese, F. *Coord. Chem. Rev.* **2009**, *253*, 526.
(76) Scalmani, G.; Frisch, M. J.; Mennucci, B.; Tomasi, J.; Cammi, R.; Barone, V. *J. Chem. Phys.* **2006**, 124.
(77) Improta, R.; Barone, V.; Scalmani, G.; Frisch, M. J. *J. Chem. Phys.* **2006**, 125.
(78) Frisch, M. J.; Trucks, G. W.; Schlegel, H. B.; Scuseria, G. E.; Robb, M. A.; Cheeseman, J. R.; Scalmani, G.; Barone, V.; Mennucci, B.; Petersson, G. A.; Nakatsuji, H.; Caricato, M.; Li, X.; Hratchian, H. P.; Izmaylov, A. F.; Bloino, J.; Zheng, G.; Sonnenberg, J. L.; Hada, M.; Ehara, M.; Toyota, K.; Fukuda, R.; Hasegawa, J.; Ishida, M.; Nakajima, T.; Honda, Y.; Kitao, O.; Nakai, H.; Vreven, T.; Montgomery, J. A.; Peralta, J. E.; Ogliaro, F.; Bearpark, M.; Heyd, J. J.; Brothers, E.; Kudin, K. N.; Staroverov, V. N.; Kobayashi, R.; Normand, J.; Raghavachari, K.; Rendell, A.; Burant, J. C.; Iyengar, S. S.; Tomasi, J.; Cossi, M.; Rega, N.; Millam, J. M.; Klene, M.; Knox, J. E.; Cross, J. B.; Bakken, V.; Adamo, C.; Jaramillo, J.; Gomperts, R.; Stratmann, R. E.; Yazyev, O.; Austin, A. J.; Cammi, R.; Pomelli, C.; Ochterski, J. W.; Martin, R. L.; Morokuma, K.; Zakrzewski, V. G.; Voth, G. A.; Salvador, P.; Dannenberg, J. J.; Dapprich, S.; Daniels, A. D.; Farkas, Ö.; Foresman, J. B.; Ortiz, J. V.; Cioslowski, J.; Fox, D. J. *Gaussian 09, Revision A.02*; Gaussian, Inc.: Wallingford, CT, 2010.
(79) Ferreira, K. Q.; Lucchesi, A. M.; da Rocha, Z. N.; da Silva, R. S. *Inorg. Chim. Acta* **2002**, *328*, 147.
(80) Alezra, V.; Bernardinelli, G.; Corminboeuf, C.; Frey, U.; Kndig, E. P.; Merbach, A.; Saudan, C. M.; Viton, F.; Weber, J. *J. Am. Chem. Soc.* **2004**, *126*, 4843.
(81) Rapaport, I.; Helm, L.; Merbach, A. E.; Bernhard, P.; Ludi, A. *Inorg. Chem.* **1988**, *27*, 873.
(82) Stebler-Roethlisberger, M.; Hummel, W.; Pittet, P. A.; Buergi, H. B.; Ludi, A.; Merbach, A. E. *Inorg. Chem.* **1988**, *27*, 1358.
(83) Bensasson, R.; Salet, C.; Balzani, V. *J. Am. Chem. Soc.* **1976**, *98*, 3722.
(84) Braterman, P. S.; Harriman, A.; Heath, G. A.; Yellowlees, L. J. *J. Chem. Soc., Dalton Trans.* **1983**, 1801.
(85) Taffarel, E.; Chirayil, S.; Kim, W. Y.; Thummel, R. P.; Schmehl, R. H. *Inorg. Chem.* **1996**, *35*, 2127.
(86) Van Houten, J.; Watts, R. J. *J. Am. Chem. Soc.* **1976**, *98*, 4853.
(87) Allsopp, S. R.; Cox, A.; Kemp, T. J.; Reed, W. J. *J. Chem. Soc., Faraday Trans.* **1978**, *74*, 1275.
(88) Durham, B.; Caspar, J. V.; Nagle, J. K.; Meyer, T. J. *J. Am. Chem. Soc.* **1982**, *104*, 4803.
(89) Norrby, T.; Börje, A.; Åkermark, B.; Hammarström, L.; Alsins, J.; Lashgari, K.; Norrestam, R.; Mårtensson, J.; Stenhagen, G. *Inorg. Chem.* **1997**, *36*, 5850.
(90) Li, C.; Hoffman, M. Z. *Inorg. Chem.* **1998**, *37*, 830.
(91) Chang, J.; Fedro, A. J.; van Veenendaal, M. *Chem. Phys.* **2012**, *407*, 65.
(92) Wasylenko, D. J.; Ganesamoorthy, C.; Henderson, M. A.; Koivisto, B. D.; Osthoff, H. D.; Berlinguette, C. P. *J. Am. Chem. Soc.* **2010**, *132*, 16094.
(93) Yoshida, M.; Masaoka, S.; Sakai, K. *Chem. Lett.* **2009**, *38*, 702.
(94) Winget, P.; Weber, E. J.; Cramer, C. J.; Truhlar, D. G. *Phys. Chem. Chem. Phys.* **2000**, *2*, 1231.
(95) Baik, M. H.; Friesner, R. A. *J. Phys. Chem. A* **2002**, *106*, 7407.
(96) Uudsemaa, M.; Tamm, T. *J. Phys. Chem. A* **2003**, *107*, 9997.
(97) Jaque, P.; Marenich, A. V.; Cramer, C. J.; Truhlar, D. G. *J. Phys. Chem. C* **2007**, *111*, 5783.
(98) Shimodaira, Y.; Miura, T.; Kudo, A.; Kobayashi, H. *J. Chem. Theory Comput.* **2007**, *3*, 789.
(99) Chiorescu, I.; Deubel, D. V.; Arion, V. B.; Keppler, B. K. *J. Chem. Theory Comput.* **2008**, *4*, 499.
(100) Schultz, D.; Biaso, F.; Shahi, A. R. M.; Geoffroy, M.; Rissanen, K.; Gagliardi, L.; Cramer, C. J.; Nitschke, J. R. *Chem.—Eur. J.* **2008**, *14*, 7180.
(101) Cramer, C. J.; Truhlar, D. G. *Acc. Chem. Res.* **2008**, *41*, 760.
(102) Galstyan, A.; Knapp, E. W. *J. Comput. Chem.* **2009**, *30*, 203.
(103) Namazian, M.; Lin, C. Y.; Coote, M. L. *J. Chem. Theory Comput.* **2010**, *6*, 2721.
(104) Zhao, Y.; Truhlar, D. G. *Rev. Mineral. Geochem.* **2010**, *71*, 19.
(105) York, J. T.; Llobet, A.; Cramer, C. J.; Tolman, W. B. *J. Am. Chem. Soc.* **2007**, *129*, 7990.
(106) Kelly, C. P.; Cramer, C. J.; Truhlar, D. G. *J. Phys. Chem. A* **2006**, *110*, 2493.
(107) Ho, J. M.; Coote, M. L. *Theor. Chem. Acc.* **2010**, *125*, 3.
(108) Alongi, K. S.; Shields, G. C. In *Annual Reports in Computational Chemistry*; Wheeler, R., Ed.; Elsevier: Dordrecht, 2010; Vol. *6*, p 113.
(109) Peverati, R.; Truhlar, D. G. *J. Phys. Chem. Lett.* **2012**, *3*, 117.